Supplementary Information

Influence of amorphous phase on coercivity in $SmCo_5$-Cu nanocomposites

Franziska Staab[a,*], and Yangyiwei Yang[b,*], Eren Foya[b], Enrico Bruder[a], Benjamin Zingsem[c,d], Esmaeil Adabifiroozjaei[e], Despoina Nasiou[e], Konstantin Skokov[f], David Koch[g], Michael Farle[c], Rafal E. Dunin-Borkowski[d], Leopoldo Molina-Luna[e], Oliver Gutfleisch[f], Bai-Xiang Xu[b], Karsten Durst[a]

[a] *Physical Metallurgy (PhM), Materials Science Department, Technical University of Darmstadt, Peter-Grünberg-Str. 2, 64287 Darmstadt, Germany*

[b] *Mechanics of Functional Materials (MFM), Materials Science Department, Technical University of Darmstadt, Otto-Berndt-Str. 3, 64287 Darmstadt, Germany*

[c] *Faculty of Physics and Center for Nanointegration (CENIDE), University of Duisburg-Essen, 47057 Duisburg, Germany*

[d] *Ernst Ruska-Centre for Microscopy and Spectroscopy with Electrons and Peter Grünberg Institute, Forschungszentrum Jülich GmbH, 52425 Jülich, Germany*

[e] *Advanced Electron Microscopy (AEM), Materials Science Department, Technical University of Darmstadt, Peter-Grünberg-Str. 2, 64287 Darmstadt, Germany*

[f] *Functional Materials (FM), Materials Science Department, Technical University of Darmstadt, Peter-Grünberg-Str. 16, 64287 Darmstadt, Germany*

[g] *Structure Research, Materials Science Department, Technical University of Darmstadt, Peter-Grünberg-Str. 2, 64287 Darmstadt, Germany*

Supplementary Note 1. Experimental Details

In the following the experimental details of the production and subsequent analyses of the $SmCo_5$-Cu nanocomposite by HPT are described. The HPT process was applied to powder blends consisting of 80 wt.% intermetallic fine-grained powder of $SmCo_5$ (Alfa Aesar) and 20 wt.% of Cu powder (99.9 %, Alfa Aesar). First the powder was precompacted by HPT by the aid of a Cu-ring, placed on the lower anvil. For this the powder was filled into the Cu-ring and compacted at room temperature at a nominal pressure of 4.5 GPa by ten oscillations of $\pm 5°$ each. In a second HPT step the consolidated discs with a diameter of 10 mm and an initial height of 1.4 mm was deformed by 100 rotations, with a rate of 2 rpm at a nominal pressure of 7.6 GPa. For microstructural investigations the sample was cut and embedded in a polymer in a way that the cross section was analysed. The samples were polished with 3 µm, 1 µm and 0.25 µm diamond-suspension followed by final polishing with a colloidal silica suspension OP-U. Backscattered electron (BSE) imaging was carried out on a high-resolution scanning electron microscope (TESCAN Mira 3). A line interception method was applied for quantitative evaluation of the $SmCo_5$-particle size following the same approach as described in [1]. The sample which was subjected to 20 rotations shows no further increase of the coercivity but a saturation and was hence selected for TEM analyses. The lamella was prepared from a region showing strong refinement of the microstructure. TEM analyses was performed by 4D scanning precession electron diffraction (SPED) on a JOEL ARM 200F TEM operated at 200 kV with a step size of 1 nm, a frequency of 100 Hz and a precession of 0.5 °. The SPED technique results in experimental nanobeam electron diffraction (NBED) patterns which were directly collected from the local nanostructure and which were compared to simulated NBED patterns of the $SmCo_5$ and the Cu phase. To generate the phase map, a template matching algorithm was utilized which assigns probability values to a set of user defined templates. To examine the sample composed of amorphous $SmCo_5$ alongside crystalline $SmCo_5$ TopSpin software was used and automated crystal orientation mapping (ACOM) was performed.

Supplementary Note 2. Micromagnetic Simulations

The free energy of a micromagnetic system can be formulated as a functional of the normalized magnetization $\mathbf{m}(\mathbf{r})$ as

$$\mathcal{F} = \int_V \left[f_{\mathrm{ex}} + f_{\mathrm{ani}} + f_{\mathrm{ms}} + f_{\mathrm{zm}} \right] \mathrm{d}V, \tag{S1}$$

*Authors contributed equally; Corresponding author

Email address: yangyiwei.yang@mfm.tu-darmstadt.de (and Yangyiwei Yang)

with

$$f_{\mathrm{ex}}(\nabla \mathbf{m}) = A_{\mathrm{ex}} \|\nabla \mathbf{m}\|^2, \tag{S2}$$

$$f_{\mathrm{ani}}(\mathbf{m}) = -K_{\mathrm{u}} \left(\mathbf{u} \cdot \mathbf{m}\right)^2, \tag{S3}$$

$$f_{\mathrm{ms}}(\mathbf{m}) = -\frac{1}{2} \mu_0 M_{\mathrm{s}} \mathbf{m} \cdot \mathbf{H}_{\mathrm{dm}}, \tag{S4}$$

$$f_{\mathrm{zm}}(\mathbf{m}, \mathbf{H}_{\mathrm{ext}}) = -\mu_0 M_{\mathrm{s}} \mathbf{m} \cdot \mathbf{H}_{\mathrm{ext}}, \tag{S5}$$

where V is the volume of the system. Here, f_{ex} is the exchange contribution, taking into account the parallel-aligning tendency between neighbouring magnetic moments due to the Heisenberg exchange interaction. f_{ani} represents the contribution of the magnetocrystalline anisotropy. The magnetostatic term f_{ms} counts the energy of each local magnetization under the demagnetizing field $\mathbf{H}_{\mathrm{dm}}$ created by the surrounding magnetization. The Zeeman term f_{zm} counts the energy of each local magnetization under an extrinsic magnetic field $\mathbf{H}_{\mathrm{ext}}$.

It is worth noting that the free energy density contributions as shown in Eqs. (S2)-(S5) with positively defined parameters, namely the exchange stiffness A_{ex}, the magnetocrystalline anisotropy constant K_{u}, and saturation magnetization M_{s}, generally describe ferromagnetic materials (in this work, both nanocrystalline and amorphous $SmCo_5$), where the spontaneous $\mathbf{m}$ exists below the Curie temperature. For diamagnetic Cu phase with a magnetic susceptibility χ, these terms are correspondingly modified as

$$f_{\mathrm{ex}}(\nabla \mathbf{m}) = 0, \tag{S6}$$

$$f_{\mathrm{ani}}(\mathbf{m}) = 0, \tag{S7}$$

$$f_{\mathrm{ms}}(\mathbf{m}) = -\frac{1}{2} \mu_0 M_{\mathrm{s}} \mathbf{m} \cdot \mathbf{H}_{\mathrm{dm}}, \tag{S8}$$

$$f_{\mathrm{zm}}(\mathbf{m}, \mathbf{H}_{\mathrm{ext}}) = -\mu_0 M_{\mathrm{s}} \mathbf{m} \cdot \mathbf{H}_{\mathrm{ext}}. \tag{S9}$$

In Fig. S1 we present the $M(H)$ behavior of the modeled diamagnetic Cu in a micromagnetic simulation.

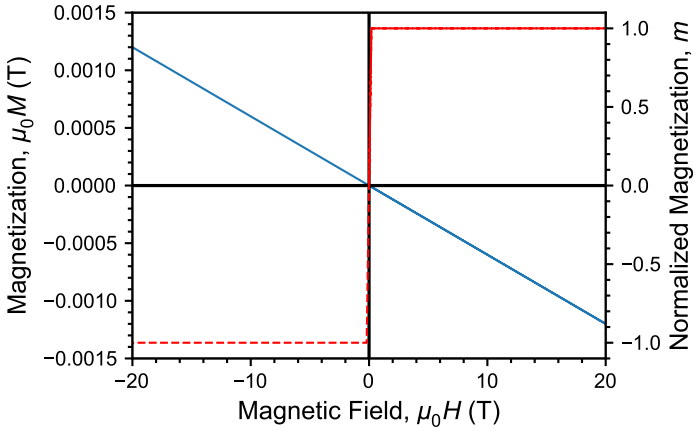

Fig. S1. Magnetization-field curve of simulated diamagnetic Cu.

The magnetization reversal under an imposed cycling magnetic field was generally described by the Landau-Lifshitz-Gilbert (LLG) equation as

$$\frac{\partial \mathbf{m}}{\partial t} = \frac{\gamma_{\mathrm{mg}}}{1 + \alpha_{\mathrm{d}}^2} \frac{1}{\mu_0 M_{\mathrm{s}}} \left[\mathbf{m} \times \frac{\delta \mathcal{F}}{\delta \mathbf{m}} + \alpha_{\mathrm{d}} \mathbf{m} \times \left(\mathbf{m} \times \frac{\delta \mathcal{F}}{\delta \mathbf{m}} \right) \right] \tag{S10}$$

with the vacuum permeability μ_0, the gyromagnetic ratio γ_{mg} and the damping coefficient α_{d} [2]. However, due to the incomparable time scale of LLG-described magnetization dynamics (around nanoseconds) with respect to the one of hysteresis measurement (around seconds), constrained optimization of the free energy functional $\mathscr{F}$ has been widely employed as a computationally efficient alternative to the time-dependent calculation in evaluating the hysteresis behavior of permanent magnets [3–5]. Based on the steepest conjugate gradient (SCG) method, the iteration scheme

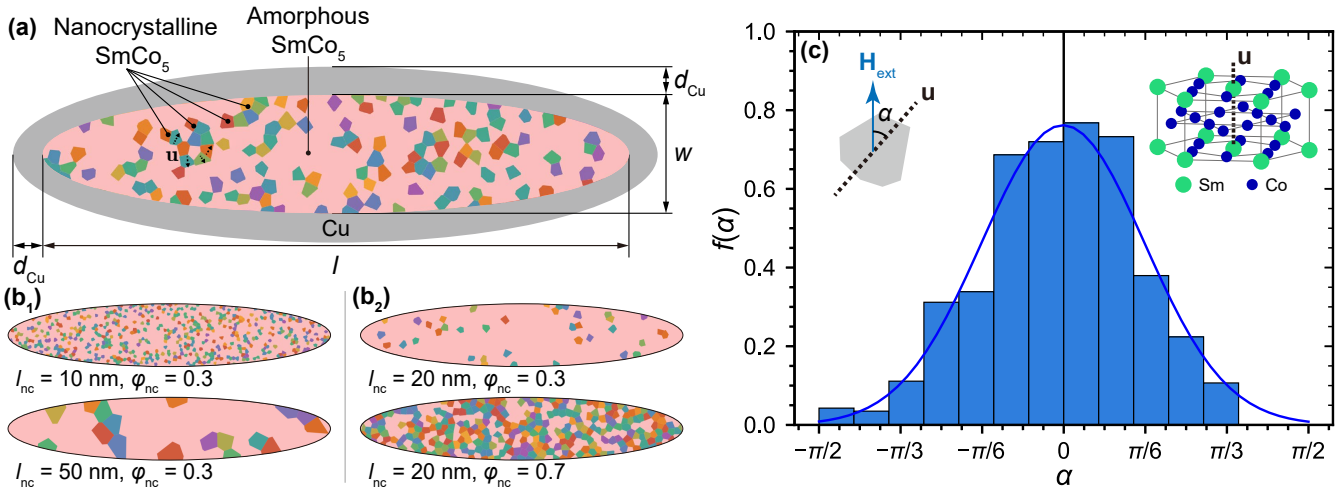

Fig. S2. (a) Schematic of the parameterized elliptical nanocomposites for micromagnetic simulations, containing $SmCo_5$ nanocrystals and the amorphous matrix. Two varying parameters are focused: (b_1) varying average nanocrystal size l_{nc} from 10 to 50 nm with fixed volume fraction $\varphi_{nc} = 0.3$; (b_2) varying φ_{nc} from 0.1 to 0.7 with $l_{nc} = 20$ nm. (c) Pre-scribed orientation angle (α) distribution for random-assignment of the nanocrystalline easy axis ($\mathbf{u}$). The probability density function $f(\alpha)$ takes the Gaussian form. The histogram of assigned α in the nanocomposite $l_{nc} = 20$ nm, $\varphi_{nc} = 0.3$ is also illustrated as an instance. Inset: definition of the angle α and schematic of the $SmCo_5$ unit cell with $\mathbf{u}$ denoted [7].

is derived as

$$\frac{\mathbf{m}^{(i+1)} - \mathbf{m}^{(i)}}{\Delta^{(i)}} = \mathbf{m}^{(i)} \times \frac{1}{\mu_0 M_s}\left[\mathbf{m}^{(i)} \times \frac{\delta \mathscr{F}}{\delta \mathbf{m}^{(i)}}\right], \quad \text{subject to} \quad |\mathbf{m}| = 1 \tag{S11}$$

with the iteration step size $\Delta^{(i)}$ and the magnetization configuration $\mathbf{m}^{(i)}$ of the step i. The iteration scheme in Eq. (S11) is in accordance with the sole damping term of the LLG equation (Eq. (S10)) [3, 5]. This also means that the magnetic hysteresis is evaluated under the quasi-static condition [3–5].

In this work, we conducted micromangetic simulations on a parameterized nanocomposite, containing an elliptical nanocomposite region with the major axis $l = 900$ nm and minor axis $w = 180$ nm (aspect ratio of 5:1), and a Cu-coated region with the thickness $d_{Cu} = 50$ nm, as shown in Fig. S2a. Nanocrystalline and amorphous $SmCo_5$ inside the nanocomposite region were created via the Voronoi tessellation on the randomly-labeled seeds. To control the size and volume fraction of generated nanocrystals, seeds with a uniform-controlled diameter were sampled based on the fast Poisson disk sampling [6]. The amount of the seeds labeled as nanocrystals was further constrained according to the imposed seed fraction. When the seeding amount is sufficiently large, the average nanocrystal size l_{nc} and nanocrystal volume fraction φ_{nc} can be then approximated by the seed diameter and the seed fraction. To investigate the effects of the nanocrystal size and of the volume fraction separately and quantitatively, φ_{nc} was fixed at 0.3 for varying l_{nc} from 10 to 50 nm with an increment of 10 nm. For varying φ_{nc} from 0.1 to 0.7 with an increment of 0.2, l_{nc} was fixed at 20 nm. In Fig. S2b we demonstrate the generated nanocomposite with either fixed l_{nc} or fixed φ_{nc}. For reference, a fully packed nanocomposite (i.e., $\varphi_{nc} = 1.0$) with a nanocrystal size of $l_{nc} = 20$ nm was also examined. The easy axes $\mathbf{u}$ of the nanocrystals were also assigned by random sampling from a Gaussian distribution of the misorientation angle α to the applied field, as shown in Fig. S2c. The mean and the standard deviation of α are $\mu_\alpha = 0$ and $\sigma_\alpha = \pi/6$, respectively, which can guarantee 99.73% of the sampled α in-between $-\pi/2$ and $\pi/2$.

The simulation domains were $1024 \times 512 \times 20$ nm^3 in size. Periodic boundary condition (PBC) was applied along the out-of-plane (z) direction by macro geometry approach [8], while Neumann boundary condition was applied on other boundaries [9]. It should be notified that the simulation domain is equivalent to a intersection of a long elliptic cylindrical structure with columnar nanocrystals, where the in-plane domain configuration and domain wall migration are mainly resolved. In that sense, the grid number along the out-of-plane direction was decreased for reduction of computational consumption. We have tested simulations with grid size of $1 \times 1 \times 1$ nm^3, $1 \times 1 \times 2$ nm^3, $1 \times 1 \times 5$ nm^3, and $1 \times 1 \times 10$ nm^3, as simulated coercivity presented in Fig. S3 for the case $\varphi_{nc} = 0.3$ and $l_{nc} = 10$ nm. This demonstrates that the simulation with $1 \times 1 \times 10$ nm^3 grid size, which is comparable to the nanocrystal size, has a

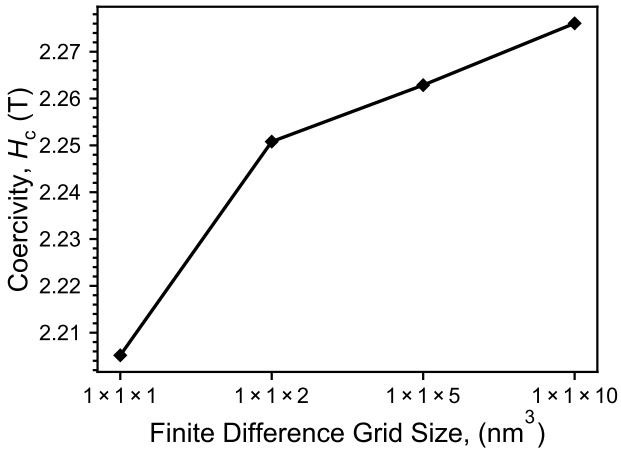

Fig. S3. Simulated coercivity of the nanocomposite with $\varphi_{\rm nc} = 0.3$ and $l_{\rm nc} = 10$ nm on varying finite element grid size.

simulated coercivity around 3.18% deviated from the one with $1 \times 1 \times 1$ nm^3 grid size. Nonetheless, it has the least computation consumption and thereby employed in this work.

Supplementary References

[1] Staab, F. *et al.* Hard magnetic $SmCo_5$−Cu nanocomposites produced by severe plastic deformation. *Acta Materialia* **246**, 118709 (2023).

[2] Coey, J. M. *Magnetism and magnetic materials* (Cambridge university press, 2010).

[3] Exl, L. *et al.* Labonte's method revisited: An effective steepest descent method for micromagnetic energy minimization. *J. Appl. Phys.* **115**, 17D118 (2014).

[4] Schabes, M. E. & Bertram, H. N. Magnetization processes in ferromagnetic cubes. *Journal of Applied Physics* **64**, 1347–1357 (1988).

[5] Furuya, A. *et al.* Semi-implicit steepest descent method for energy minimization and its application to micromagnetic simulation of permanent magnets. *IEEE Transactions on Magnetics* **51**, 1–4 (2015).

[6] Bridson, R. Fast poisson disk sampling in arbitrary dimensions. *SIGGRAPH sketches* **10**, 1 (2007).

[7] Gutfleisch, O. High-temperature samarium cobalt permanent magnets. *Nanoscale magnetic materials and applications* 337–372 (2009).

[8] Fangohr, H. *et al.* A new approach to (quasi) periodic boundary conditions in micromagnetics: The macrogeometry. *J. Appl. Phys.* **105**, 07D529 (2009).

[9] Vansteenkiste, A. *et al.* The design and verification of mumax3. *AIP Adv.* **4**, 107133 (2014).